PROCESSING OF COMMINGLED YARNS IN 3D SKELETON WINDING (3DSW)

Beck, B.[1]*, Shim, Y.-B.[2], Haas, J.[1], Eyerer, P.[1], Park, Y.-B.[2], and Henning, F.[1,3]
[1] Polymer Engineering Dept., Fraunhofer Institute for Chemical Technology (ICT), Pfinztal, Germany
[2] Mechanical Engineering Dept., Ulsan National Institute of Science and Technology (UNIST), Ulsan, South Korea
[3] Lightweight Technology Dept. at Institute of Vehicle System Technology (FAST), Karlsruhe Institute of Technology (KIT), Karlsruhe, Germany
* Corresponding author (bjoern.beck@ict.fraunhofer.de)

Keywords*: 3D filament winding, commingled yarns, overmolding*

ABSTRACT

3D skeleton winding (3DSW) enables the robot-based processing of commingled yarns (CY) to fiber skeleton structures that can be used as local continuous fiber reinforcements in structural injection molded components. This paper presents the latest version of the developed 3DSW prototype line and shows how PPS/GF CY can be processed into loop structures. This includes the investigation of the impregnation quality on different loop sections as well as the study of additional convective heating of the 3D winding area on the achievable tensile failure loads. In addition, compression shear strength test specimens are used to investigate how preheating of CY can increase the adhesion to the injection molding matrix.

1 Introduction

By integrating the right material in the smallest possible quantity at the right component areas, composites can contribute to achieve an economical lightweight design. In this context, fiber-reinforced plastics offer the characteristics of an ideal lightweight material providing high strength and stiffness combined with low densities compared to other conventional construction materials. At the same time, these materials enable the use in a functionally optimized manner, while the degree of anisotropy can be adapted to given load cases [1, 2]. In recent years, especially continuous fiber-reinforced thermoplastics were brought into focus based on an increasing number in large scale automotive applications. The lightweight potential of such components can be further maximized by systematically using local continuous fibers exclusively in the highly loaded component areas according to the occurring load paths.

Filament winding is one way to process continuous fiber-reinforced semi-finished products to semi-structural and structural components. Generally, filament winding can be classified into two main categories: conventional and robot-based filament winding [3]. In robot-based filament winding, additional degrees of freedom of a multi-axis industrial robot can be used to process continuous fibers into rather complex, non-rotationally symmetrical components. Whereas in conventional filament winding mainly rotationally symmetrical components, such as pressure vessels, axles, rollers, and tubes are produced by means of fiber deposition on a winding core, robot-based filament winding can be carried out with and without a winding core, which significantly increases the complexity of producible components.

Within coreless 3D filament winding processes, 3D skeleton winding (3DSW) presents a novel manufacturing method to process thermoplastic CY to fiber skeleton structures [4, 5]. The use of component-specific winding tools allows the robot-based 3D winding of impregnated continuous fibers around hard points or load introduction

elements (e.g., aluminum inserts). By embedding such hybrid skeleton structures using conventional injection molding, it is possible to locally reinforce structural thermoplastic components with continuous fibers. To maximize the component's lightweight potential, the continuous fibers are introduced exclusively in the highly stressed component areas according to the critical load paths identified by means of topology optimizations. Compared to consolidated unidirectional tape-layups or organo sheets, which can generally also be used as local continuous fiber reinforcements in injection molding, the use of CY provides higher flexibility leading to higher possible complexities of the continuous reinforcement structure. At the same time, offcuts are kept at a minimum, which is in line with the efficient use of resources. A high degree of automation enables the manufacturing of fiber skeletons in injection molding typical cycle times. This means that the developed technology can also be used economically for highly optimized structural components in high-volume applications (e.g., in the automotive industry).
Although thermoset semi-finished materials can in principle also be processed in 3DSW, the developed prototype line is designed for processing thermoplastic semi-finished materials (e.g., CY). CY typically consist of thermoplastic matrix filaments and reinforcing fibers (e.g., glass, carbon, or aramid fibers) that are textured or intermingled. During air texturing, the individual filaments are fed with different feed rates to an air nozzle in which the components are opened by means of cold or hot compressed air and commingled with one another in an air stream [6]. Fiber volume contents are typically between 30 and 60 vol.%. By mixing the thermoplastic matrix filaments and reinforcing fibers already prior to processing, the highly viscous thermoplastic matrix (100 - 5000 Pas) only needs to cover short flow path during the impregnation [1, 6–8].

2 3DSW process development

In recent years, coreless robot-based filament winding methods have been presented in several research studies. For instance, Minsch et al. developed a filament winding process in which two collaborating robots can manufacture 3D struss structures from carbon fibers impregnated with a thermoset resin system [9]. A similar approach with collaborating 6-axis industrial robots was presented by Sbanca et al. [10]. Prado et al. reported an innovative thermoset-based coreless 3D filament winding approach using a 12-axis robotic system with two synchronized industrial robots to produce building and construction elements [11]. Automated manufacture of large truss structures is also enabled by a 11-axis robotic gantry system developed by Büchler et al. [12].
The different coreless 3D filament winding processes have in common that they can generally be distinguished in their type of strand guidance and winding tool manipulation. Figure 1 illustrates the possible 3D filament winding approaches: (a) robot-manipulated fiber guide - stationary winding tool position; (b) stationary fiber guide - robot-manipulated winding tool position; (c) robot-manipulated fiber guide - robot-manipulated winding tool position.

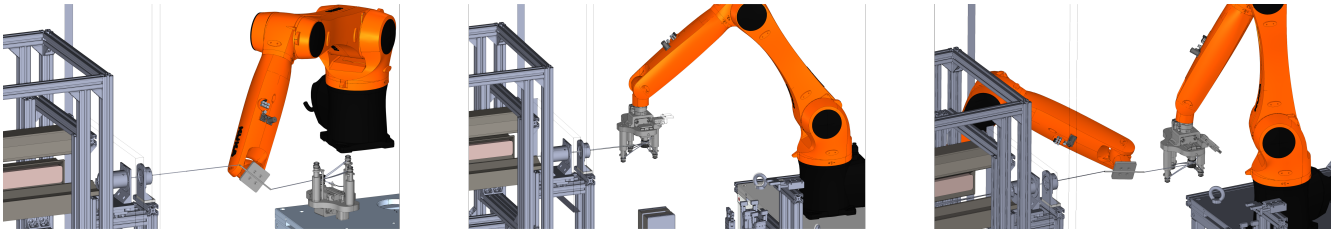

Figure 1: Process variants of coreless 3D filament winding processes: (a) robot-manipulated fiber guide - stationary winding tool position (left); (b) stationary fiber guide - robot-manipulated winding tool position (middle); (c) robot-manipulated fiber guide - robot-manipulated winding tool position (right)

The winding approach in 3DSW is based on process variant (b) (cf., Figure 1), in which the fiber guide is realized stationary, while the winding tool is robot-manipulated. This process variant is characterized by fiber-friendly processing of the CY. By using the degrees of freedom of a 6-axis robot, fiber deflections at the fiber guide can be

kept significantly lower compared to process variant (a). Process variant (b) additionally offers the possibility of setting up a stationary heating unit for the processing of thermoplastic semi-finished products and carrying out tool manipulation at a nearly constant distance from the fiber guide. As a result, process variant (b) facilitates keeping the temperature in the deposit area at a constant level, which is of particular importance when processing thermoplastic-based semi-finished products. While the robot programming for the translatory robot movements in process variant (a) can be implemented with common teach-in methods, the robot trajectory generation for complex rotational movements in process variant (b) is significantly more complex and time-consuming. An additional fiber-guiding robot, as given in process variant (c), further increases the robot programming effort, while also enabling the production of structures with higher complexity.

The developed 3DSW can be divided into the three sub-process steps: "heating and impregnation"; "robot-based 3D winding"; and "overmolding of fiber skeletons". The sub-process step "heating and impregnation" is in principle like the general setup of a thermoplastic pultrusion line in which, depending on the configuration, CY can also be processed as semi-finished products. However, compared to conventional pultrusion, the processing of CY in 3DSW cannot be considered a continuous process, as the subsequent processes "robot-based 3D winding" and "overmolding of fiber skeletons" are discontinuous with individual cycle times. In 3DSW, the CYs to be processed are taken up by a creel from where they are pulled through an infrared (IR) heating unit heating the thermoplastic filaments of the CY above melting temperature. The IR heating section consists of three IR modules arranged in an inverted U-shape, each consisting of three ceramic hollow chamber IR panel radiators. The IR heating unit is followed by a heated consolidation nozzle, in which the final fiber impregnation and the combination of the individual rovings into one strand takes place. The cross-section of the strand is defined by the nozzle geometry, whereby a round nozzle with a diameter of 2 mm was used for this study. Downstream the consolidation nozzle, a heated fiber guide eyelet (diameter 2.5 mm) serves as a reference point for the robot-based winding according to process variant (b). Fiber pretensioning, which is generally decisive for robot-based filament winding and the component quality, is determined by a pneumatically regulated braking force on the coil carrier of the creel as well as by the filling level-dependent friction forces in the nozzle. The 3D winding area begins immediately after the strand guide eyelet. To keep the strand above melting temperature until the fiber is fully deposited on the winding tool, two hot air blowers are integrated in the heating line to enable convective temperature control of the 3D winding area. An illustration of the developed heating line is given in Figure 2 (left).

A KUKA AGILUS KR10 R1100 sixx is used for the robot-based winding tool manipulation. To apply 3D winding process variant (b) (cf. Figure 1), the software-limited rotation range of the sixth axis was modified to enable infinite rotation. The winding tool attached to the robot flange corresponds to the fiber skeleton to be produced. It contains a pneumatic gripper for CY gripping and cylindrical holders for the metallic load introduction elements (aluminum inserts). The inserts are provided by an insert magazine and picked up by the robot prior to the winding sequence. A pneumatically driven vertically movable gripper cutting unit provides the CY material at the beginning of the winding cycle. Since the CY material is not pulled off any further between two winding cycles (discontinuous process), the material in the nozzle at standstill must first be pulled out and removed to avoid any degraded material in the wound fiber skeleton. Immediately after the offcut is removed the robot manipulates the winding tool in a rapid traverse to the initial strand pick-up position to take over the molten CY strand from the gripper cutting unit. After completion of the winding sequence, the gripper cutting unit takes over the strand as before and cuts it from the wound fiber skeleton. The fiber skeleton can finally be ejected as soon as the CY is solidified (10-30 s - depending on the winding number). The winding sequence is illustrated in Figure 2 (right).

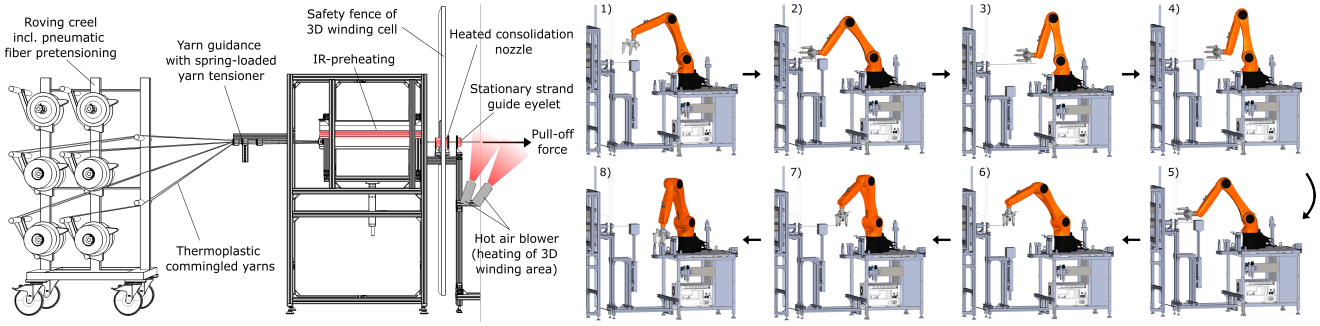

Figure 2: Sub-process step “heating and impregnation” (left); Sub-process step “robot-based 3D winding” (right): 1) home position, 2) initial strand pick-up position, 3) linear pull-off of degraded material, 4) gripping and cutting of strand, 5) clamping of new strand material, 6) 3D winding, 7) gripping and cutting of strand after 3D winding, 8) ejection of fiber skeleton

The final sup-process step “overmolding of fiber skeleton structures” involves the embedding of the wound fiber skeleton and the realization of the final component geometry using conventional injection molding. In general, identical, or compatible thermoplastic matrix systems are considered for both CY and overmolding matrix. To exploit the full potential of local continuous fibers, they are ideally integrated in component areas subjected to tensile stress. Component stresses occurring transverse to the fiber direction, compressive stress in the longitudinal fiber direction and general shear stress must be taken up by the injection molding matrix [1].
The modular design of 3DSW allows an easy integration into existing manufacturing environments. While the 3D winding robot is responsible for the fiber skeleton production, a handling robot of a conventional injection molding setup can perform the insertion of the fiber skeleton into the mold as well as the removal of the final component after the cooling time has elapsed. During the overmolding step the 3D winding robot can already produce the next fiber skeleton. Therefore, it is particularly important that the cycle time of 3D winding (depending on winding complexity and number of windings) matches the cycle time of the overmolding step. The entire process chain of the 3DSW prototype line is illustrated in Figure 3.

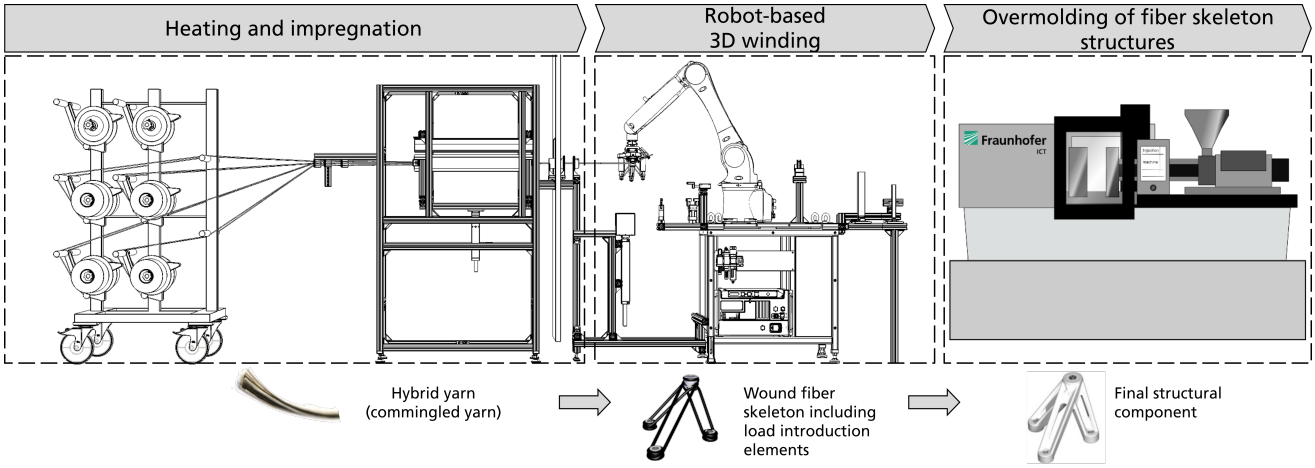

Figure 3: 3DSW process chain

3 Materials and methods

The investigations are carried out using generic tensile loop specimens. Therefore, a winding tool adapted to the shape of the loop specimen including two insert holders with a center distance of 120 mm is used. The insert holders

of the winding tool include spring-loaded pressure pins to ensure that the inserts can be picked up by the robot automatically without further fastening mechanisms. This also offers the possibility of automated removal of the wound fiber skeleton structure after the winding sequence, which is necessary for process automation. Each wound test specimen is produced with a pull-off speed of 2 m/min. The consolidation nozzle and the strand guide eyelet are operated at 400 °C. Depending on the strand diameter and pull-off speed, the set temperature at the nozzle needs to be set well above the melting temperature of the processed thermoplastic filament to ensure complete volumetric melting due to the short dwell time in the nozzle.
As standard semi-finished product, a 600 tex CY from Comfil ApS (type 50G-PPS-600 containing Celanese FORTRON® 0214 PPS filaments) is used. It contains 50 wt.% E-glass fiber of a multi-purpose roving grade with PPS-suitable silane sizing (NEG TufRovTM 4588). In addition, a PPS/GF CY (type 50G-PPS-U3020-600) was developed together with Comfil ApS, whereas the commingled PPS filaments are made from an impact modified PPS (DSM Xytron™ U3020E) to increase the elongation at break compared to the standard PPS material from 3 to 9 % [13, 14]. To ensure comparability, this CY is made in the same yarn count (600 tex) with the same glass fiber type (NEG TufRovTM 4588) and content (50 wt.%). For overmolding the same impact modified PPS (DSM Xytron™ U3020E) is used without any further short fiber reinforcements. The specimen used is illustrated in Figure 4.

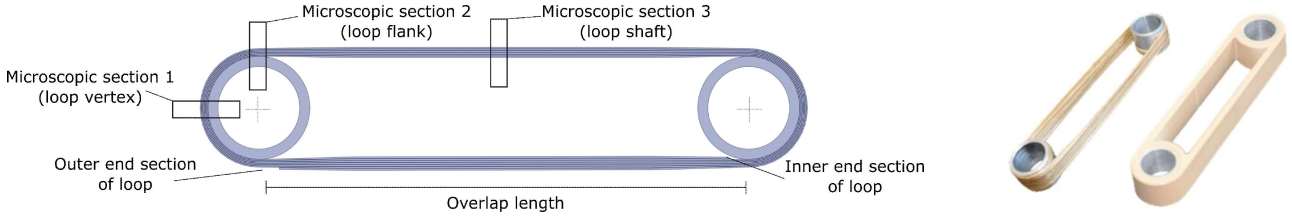

Figure 4: Tensile loop test specimen including illustration of sections for microscopic investigation (left); Tensile loop test specimen: PPS/GF fiber skeleton structure before / after overmolding (right)

The porosity investigation of wound loop structures is conducted at three characteristic sections (microscopic section (MS) 1-3), as shown in Figure 4 (left). The impregnation quality is assumed to vary between loop vertex, loop flank, and loop shaft as the strands are compacted to different degrees during the deposition. To investigate the porosity, the loops are cut at MS 1-3, embedded in mounting resin, and then polished with SiC papers and diamond lubricants. The investigation is performed for both CY materials at 2, 4 and 6 windings unsing SEM images (Zeiss Supra 55 VP) at 40x magnification and 1024x768 pixels. Individual SEM images are merged to allow the complete strand cross-section to be evaluated. Larger gaps between the individual strands occurring occasionally in MS3 are not defined as voids. The SEM images obtained are subsequently imported into MATLAB and processed in several steps: 1) conversion to a gray image; 2) counting the pixels in gray levels; 3) drawing the histogram of the pixels; 4) determining threshold values; 5) adding up pixels between the thresholds; 6) calculating the volume fractions. For the second step, counting pixels in gray levels, the ‘imhist’ function of the MATLAB image processing toolbox was used. The thresholds in the fourth step can be determined as the minimum values of each valley in the gray scale histogram. The volume fraction of the fibers and matrix, as well as the void content, can be determined by adding up the respective pixels in relation to the total number of pixels of the strand’s cross-section. Several articles refer to the gray scale method for area measurement being less accurate than the fiber counting method [15]. However, since the fibers and thermoplastic filaments in the CY are not homogeneously dispersed over the cross-section, fiber-rich and matrix-rich areas are obtained in the processed strand. This requires a low magnification to investigate the total cross section, which is not suitable for the fiber counting method. Figure 5 shows the SEM cross-sectional images as well as the evaluated gray area exemplarily for 2 windings on MS 2 with impact modified PPS/GF CY material.

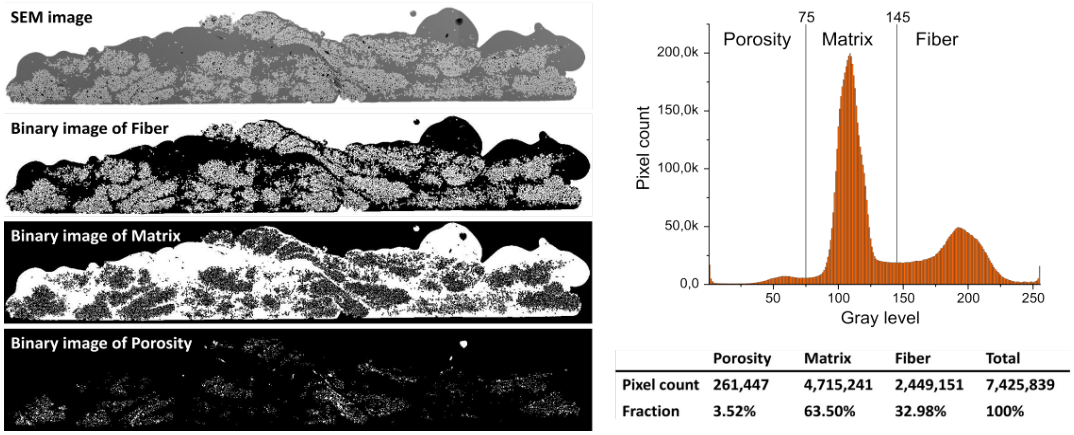

	Porosity	Matrix	Fiber	Total
Pixel count	261,447	4,715,241	2,449,151	7,425,839
Fraction	3.52%	63.50%	32.98%	100%

Figure 5: Exemplary illustration of the strand cross-section (left); gray level evaluation (right)

Furthermore, fiber skeleton loop test specimens as well as the overmolded loop test specimens are characterized using a universal testing machine (Hegewald & Peschke Inspekt table 50). At least seven test specimens per parameter setting are tested using a test speed of 5 mm/min. The test force is applied to the loop structure by means of a bolt in a test fixture attached to the upper crosshead of the testing machine. Another bolt connects the second insert firmly to the test fixture at the lower crosshead of the testing machine.

When overmolding wound fiber skeletons, an interface is obtained between the injection molding matrix and the CY of the fiber skeleton. To investigate the interfacial strength between the two components compression shear strength tests are carried out as a function of different CY preheating temperatures. Therefore, plates are press-consolidated from standard PPS/GF CY, from which small specimens are milled out and placed in a metal sheet pattern. Subsequently the PPS/GF specimens are preheated to three different temperature levels ($T_1<T_M$; $T_2\approx T_M$; $T_3>T_M$) and overmolded with PPS (DSM Xytron^{TM} U3020E) using a flow spiral injection mold. The flow spiral mold installed on a KraussMaffei 550-2000GX injection molding machine enables the characterization of the compression shear strength at different flow path lengths (s_{FP1} = 63 mm; s_{FP2} = 303 mm; s_{FP3} = 779 mm; s_{FP4} = 1005 mm). By using an IR heating unit attached to a handling robot (KUKA KR90 R2700 pro) reproducible preheating of the PPS/GF specimens prior to overmolding is ensured. The injection molding parameters are kept constant with an injection speed of 30 cm³/s, a mold temperature of 150 °C and a cooling time of 45 s. Using the flow spiral mold with a maximum flow distance of 1800 mm, it is not possible to fill the cavity over the entire length without reaching the machine's maximum injection pressure. Therefore, the injection pressure was limited to 800 bar, so that in case of a freeze up of the melt front before reaching the switchover point, the melt front does not break up due to excessive pressure on the plastic core, which might influence the validity of the results. The production and testing of the compression shear strength specimens is given in Figure 6.

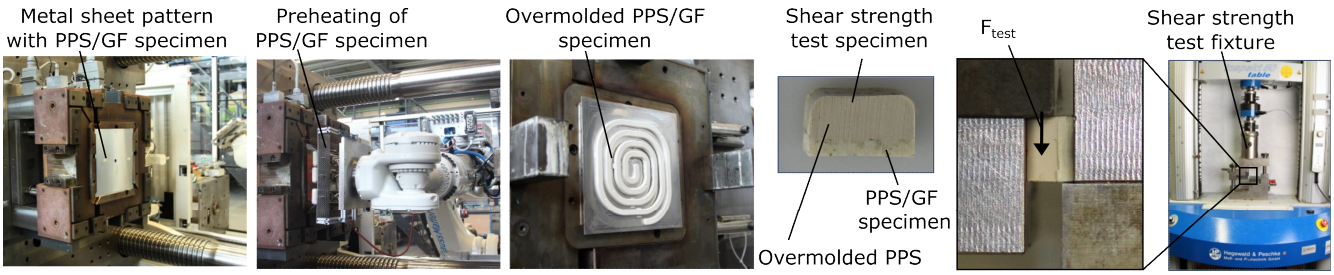

Figure 6: Manufacturing and testing of PPS/GF compression shear strength specimen [16]

4 Experimental results and discussion

4.1 Investigation of the impregnation quality of PPS/GF CY

The impregnation quality of tensile loop specimens was qualitatively investigated at three characteristic loop sections. The fiber and matrix volume fraction as well as the void content was measured, as given in Figure 7. According to the data sheets of the CY manufacturer, the fiber and matrix volume fraction is 34.0% and 66.0%, respectively. The measured fiber volume fraction was on average 3.79% below the manufacturer's specification for all samples, whereas the matrix volume fraction was on average 0.19% above the manufacturer's specification. As assumed, the porosity differs between the three different loop sections. Independently of the winding number, MS3, where the strands are not explicitly deposited on an insert surface, showed on average the highest void content of 6.95% and 6.15% for the two CY materials across all analyzed specimens (cf. Fig. Figure 7 (right)). This can be related to a lack of compaction pressure of the individual layers during deposition in MS3. At the same time, an increase in the winding number tended to decrease the void content at MS3. However, despite the highest void content being in this loop section, failure of the manufactured loops occurred invariably at MS2, where the highest stresses usually occur in loop connections under tensile load [1]. Thus, the pore content at the failure-critical MS2 should be particularly minimized in loops under tensile load to maximize the load-bearing capacity. At 3.28 % and 2.9 %, the average void content in MS2 was at a similar level for both CY materials used within this investigation.

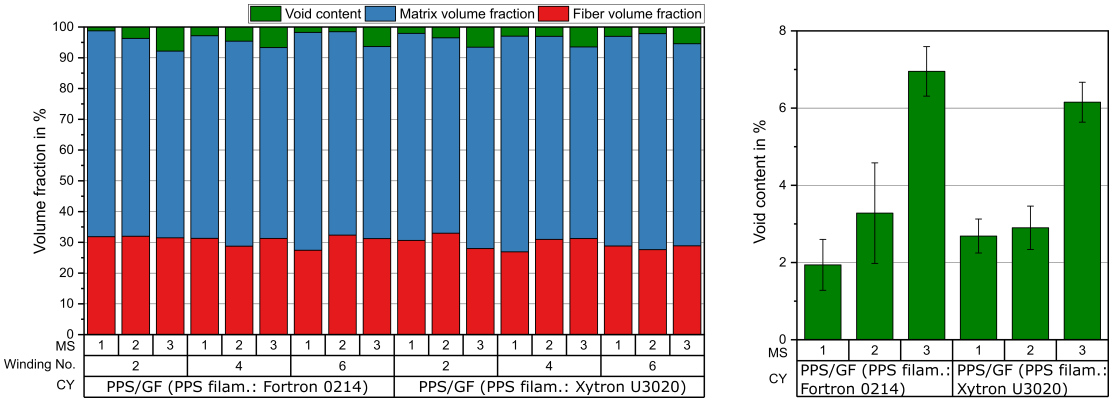

Figure 7: Fiber/matrix volume fraction and void content (left); average void content by sections (right)

4.2 Tensile testing of simple loop test specimens manufactured in 3DSW

The mechanical performance of PPS/GF loop structures was characterized under tensile load using overmolded and non-overmolded specimens (cf. Figure 4 - right). To ensure strand temperatures above T_M = 280 °C during 3D winding, the winding area was extended by two hot air blowers that can be operated up to 600 °C set temperature. Figure 8 shows how a convection heated winding area increased the failure load of non-overmolded loop structures with 2, 4 and 6 windings by 28%, 13% and 10% for the standard CY (PPS/GF with Fortron 0214 PPS filaments). For the CY containing impact modified PPS (PPS/GF with Xytron U3020 PPS filaments), the increase in failure load related to convection heating was measured with 26%, 19% and 10% for 2, 4 and 6 windings, respectively. While thermoset-based semi-finished products can be generally wound without any additional heating in the winding area, heating the winding area has a direct effect on the mechanical performance when using CY based on thermoplastics. As known from the investigations from Huber and Haas et al. [17–19], non-overmolded loop structures with low winding numbers may fail prematurely under tensile load due to local or complete delamination. The results obtained indicate that the contact area of the individual windings can be increased when using a convection heated winding area (lower PPS viscosity/higher strand flexibility during deposition). An increased contact area helps to

increase the failure load especially with low numbers of windings, since the risk of delamination and subsequent unwinding is rather reduced as the number of windings increases [17]. This agrees with the fact that the positive influence of convection heating in the winding area is higher for those non-overmolded samples that have low winding numbers. The lower performance of non-overmolded loops made from the impact modified CY can be related to the generally lower properties of the impact modified PPS compared to the standard PPS matrix in the respectively processed CY (e.g., tensile stress at break: 90 MPa (Fortron 0214); 60 MPa (Xytron U3020) [13, 14]).
For fiber skeletons overmolded with impact modified PPS (Xytron U3020), it should be noted that the risk of delamination of the individual layers is reduced by the overmolded matrix. This led to the fact that the positive effect of convection heating observed on non-overmolded specimens could not be seen in the overmolded specimens' test series. In case of processing CY with E-glass fibers (elongation at break 3.3 – 4.8 % [6]) and applying the tensile load on the continuous glass fibers in a form fit manner (loop connection), however, insufficient ductility of the PPS matrix in the CY (Fortron 0214: 3% elongation at break [13]) can lead to premature failure in case the general risk of delamination of the individual layers is prevented by the overmolding matrix. It can be assumed that this premature failure is initiated by matrix failure in the CY. By using impact modified PPS (Xytron U3020: 9% elongation at break for [14]) for both CY and overmolding, it is possible to transfer the load entirely into the continuous fibers achieving fiber failure at the failure-critical loop section (loop flank). In this case it was possible to increase the failure load up to 36.8%, 88.2% and 113.5% by adding 2, 4 and 6 windings (equal to a calculated fiber content of approx. 3.2 wt.%, 5.8 wt.%, 8.3 wt.%) compared to unreinforced injection molded reference samples (Ref.). Even though the matrix portion resulting from the glass fiber-based CY in the overall component is low (depending on the winding number and component geometry), the elongation at break of the matrix in the CY should also be adapted to the elongation at break of the fibers to exploit the full potential of the continuous reinforcements. As generally common for fiber-reinforced plastics the elongation at break of the matrix in the CY should be approximately twice the fiber elongation at break [1].

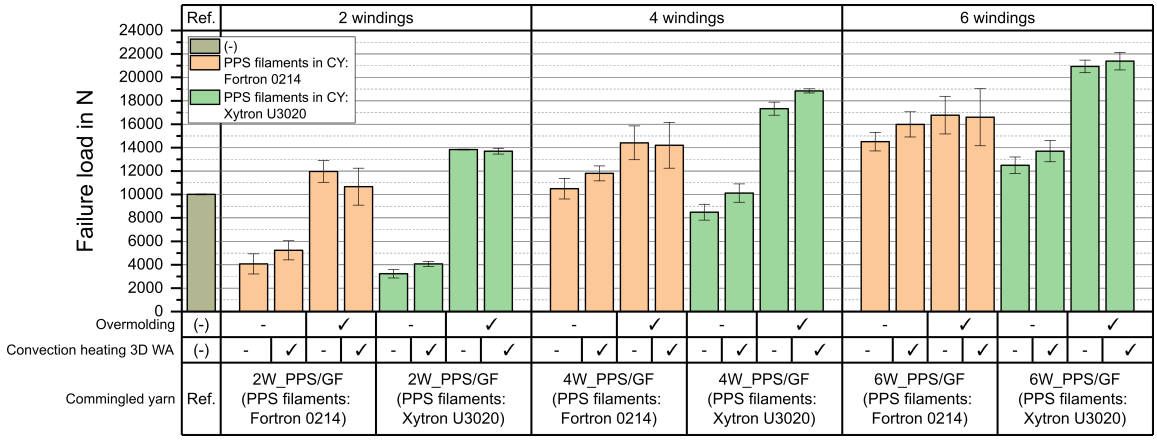

Figure 8: Tensile test results of simple loop test specimens

4.3 Characterization of adhesion between PPS/GF commingled yarns and overmolded PPS matrix

Consolidated PPS/GF CY specimens were overmolded at three different preheating temperatures and four different flow path positions (s_{FP1} - s_{FP4}) to investigate the temperature and flow path-dependent interfacial strength. Due to the hot press-based consolidation process at 20 bar surface pressure, the surface quality of the PPS/GF specimens is higher compared to PPS/GF CY processed in 3DSW. Therefore, the conducted study primarily characterized the general bonding capability of the PPS/GF CY to the PPS overmolding matrix. The preheating temperature levels were defined as three holding times of the robot-manipulated IR emitter to heat the specimens in the open mold cavity prior to overmolding ($t_{Temp.1}$ = 50 s; $t_{Temp.2}$ = 60 s; $t_{Temp.3}$ = 70 s). After the holding time has elapsed it takes 4 s to

manipulate the IR emitter out of the cavity. An additional 11.5 s (mold closing 7.6 s; bar retraction + clamping force build-up 1.53 s; aggregate forward 1.52 s; nozzle opening 0.86 s) are needed until the PPS melt is injected into the cavity. The average measured surface temperature of the preheated PPS/GF specimens in the cavity at the start of mold filling resulted in $T_{StartIM\_t1}$ = 252.2 °C, $T_{StartIM\_t2}$ = 279.0 °C and $T_{StartIM\_t3}$ = 303.0 °C for the three different holding times ($t_{Temp.1}$ - $t_{Temp.3}$). While the melt enthalpy of the injected PPS was not sufficient to realize adhesion in the interfacial area for non-preheated PPS/GF specimens, it was possible to increase the adhesion by preheating the specimens to $T_{StartIM\_t1}$ = 252.2 °C leading to an averaged shear strength of 21.9 MPa at the first flow path position (s_{FP1}), as given in Figure 9. While s_{FP2} and s_{FP3} showed similar shear strengths of approx. 16 MPa, the average shear strength at s_{FP4} dropped to 10.1 MPa with relatively high scatter.
When preheating the PPS/GF specimens for $t_{Temp.2}$ = 60 s, the surface temperature at the beginning of mold filling is in the range of the melting temperature of the injected PPS (T_M = 280 °C). Compared to the first preheating level, the shear strength was increased by approx. 29% to 28.3 MPa at s_{FP1}. Moreover, the shear strength decreased only by 3% until the flow path position s_{FP3} was reached. Only at s_{FP4} the averaged shear strength was decreased to approx. 20 MPa while the scattering increased.
For a preheating time of $t_{Temp.3}$ = 70 s, the surface temperature of the PPS/GF specimen at the start of mold filling was only approx. 20 °C degrees below the nozzle set temperature of the injection molding machine (T_N = 320 °C). Here, the shear strength increased by 26% to 35.6 MPa compared to $t_{Temp.2}$ = 60 s at s_{FP1}. The average shear strength was thus only approx. 4 MPa below the shear strength of pure injection molding material (cf. Figure 9 - Reference). These reference specimens were produced and tested without a shear strength-reducing interface (only injected Xytron U3020). Using an injection speed of 30 cm³/s it takes 2 s for the injected PPS to reach s_{FP4} leading to a temperature decrease of approx. 5 °C between s_{FP1} and s_{FP4}. Therefore, compared to the other temperature levels, $t_{Temp.3}$ = 70 s enabled that the last PPS/GF specimen at s_{FP4} was still above T_M when the injected PPS reached the PPS/GF specimen surface, which can be identified as the main reason for the high shear strength value at s_{FP4}. However, also for $t_{Temp.3}$ = 70 s the shear strength values tended to show a decrease along the flow path. This can be related to the fact that the injected PPS melt front cools down over the flow path lengths along the cold mold cavity (T_{Mold} = 150 °C). Since fiber skeletons generally show a higher surface roughness compared to the press-consolidated PPS/GF specimens investigated in this study, a higher proportion of micro form-fit bonding can be assumed. This would further increase the adhesion between the fiber skeleton and the overmolded matrix.

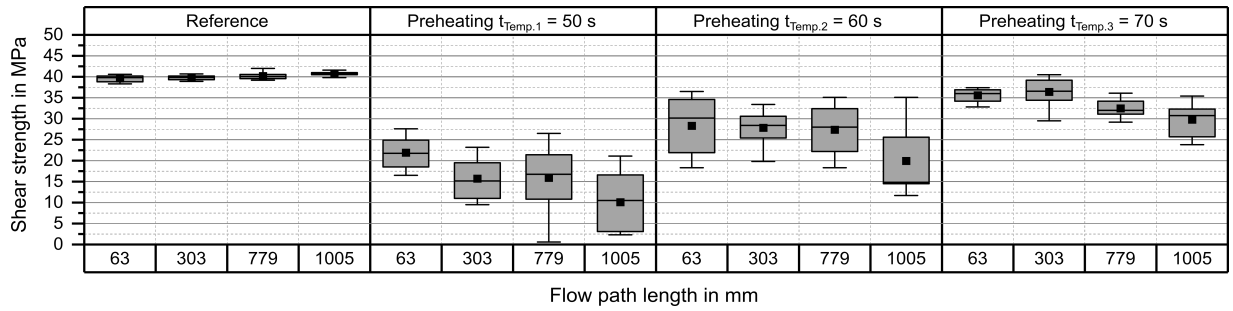

Figure 9: Compression shear strength of overmolded PPS/GF specimens at different preheating temp. and flow path positions (box 25%~75%; range with 1.5IQR; median line; mean square)

5 Conclusion

This paper presented the latest version of the developed 3DSW prototype line which can be used to produce local continuous fiber reinforcements for injection molded components. The porosity of wound loop specimens was investigated by SEM and gray level image analysis. Significantly higher void contents were found in areas where the

strand of a fiber skeleton is not deposited on an insert surface. The two investigated CY materials showed no significant difference in their porosity. Furthermore, it was possible to demonstrated that additional convection heating in the winding area is particularly important for non-overmolded fiber skeletons tested on tensile stress. At the same time, the investigations showed that the PPS matrix elongation at break of the CY needs to be increased when processing glass fibers as continuous reinforcements while overmolding the fiber skeleton with impact modified PPS. By preheating the PPS/GF material prior to overmolding, the interfacial strength between the CY and the overmolded PPS could be particularly increased when preheating the samples above melting temperature.

6 Acknowledgement

The present work is part of the VIP+ ELeGanz-3D project funded by the German Federal Ministry of Education and Research (Grant No. 03VP06670).

7 Literature

[1] H. Schürmann. *"Konstruieren mit Faser-Kunststoff-Verbunden"*. Springer, 2005.
[2] H.-H. Braess. *"Vieweg Handbuch Kraftfahrzeugtechnik"*. 6th edition, Vieweg + Teubner, 2011.
[3] J. Fleischer, R. Teti, G. Lanza et al. *"Composite materials parts manufacturing"*. CIRP Annals 67, No. 2, pp 603-626, 2018.
[4] B. Beck, J. Haas, H. Tawfik. *"Three-dimensional fiber skeleton – local continuous fiber-reinforcement through 3D skeleton winding technology"*. Kunststoffe international, 09/2019, pp 114-116, 2019.
[5] B. Beck, H. Tawfik, J. Haas et al. *"Automated 3D skeleton winding process for continuous-fiber-reinforcements in structural thermoplastic components"*. Advances in Polymer Processing 2020, pp 150-161, 2020.
[6] C. Cherif *"Textile Werkstoffe für den Leichtbau – Techniken - Verfahren - Materialien – Eigenschaften"*. Springer, 2011.
[7] F. Henning, E. Moeller. *"Handbuch Leichtbau – Methoden, Werkstoffe, Fertigung"*. Hanser, 2011.
[8] G.W. Ehrenstein. *"Faserverbund-Kunststoffe – Werkstoffe - Verarbeitung – Eigenschaften"*. Carl Hanser Verlag, 2006.
[9] N. Minsch, M. Müller, T. Gereke et al. *"Novel fully automated 3D coreless filament winding technology"*. Journal of Composite Materials 52, No. 22, pp 3001-3013, 2018.
[10] M.P. Sbanca, G.L. Mogan. *"Winding of carbon wire composite structures using two cooperative industrial robots"*. Applied Mechanics and Materials 762, pp 291-298, 2015.
[11] M. Prado, M. Dörstelmann, T. Schwinn et al. *"Core-less filament winding"*. Robotic Fabrication in Architecture, Art and Design 2014, pp 275-289, 2014.
[12] D. Büchler, T. Elsken, N. Glück et al. *"Ultraleichte Raumzelle – Entwicklung von ultraleichten Großstrukturen in Faserverbund- und Hybridbauweise für den Schiffbau"*. Tagungsband der Statustagung 2011. Forschungszentrum Jülich GmbH, pp 25-45, 2011.
[13] Celanese. *"Technical datasheet - Fortron® 0214 – PPS"*. 2019.
[14] DSM. *"Eigenschaftsdaten - Xytron™ U3020E"*. 2021.
[15] M.T. Cann, D.O. Adams, C.L. Schneider. *"Characterization of Fiber Volume Fraction Gradients in Composite Laminates"*. Journal of Composite Materials 42, No. 5, pp 447-466, 2008.
[16] K.A. Weidenmann, B. Haspel and L. Baumgärtner. *"Vorrichtung und ein Verfahren zur Bestimmung der Scherfestigkeit und des Schermoduls von Verbundwerkstoffen"*. EP 3 073 244 B1, 2016.
[17] T. Huber. *"Einfluss lokaler Endlosfaserverstärkungen auf das Eigenschaftsprofil struktureller Spritzgießbauteile"*. Wissenschaftliche Schriftenreihe des Fraunhofer ICT, Vol. 60, Fraunhofer Verlag, 2014.
[18] J. Haas, O.N. Hassan, B. Beck et al. *"Systematic approach for finite element analysis of thermoplastic impregnated 3D filament winding structures – general concept and first validation results"*. Composite Structures 268, No. 113964, 2021.
[19] J. Haas, D. Aberle, A. Krüger et al. *"Systematic approach for finite element analysis of thermoplastic impregnated 3D filament winding structures—advancements and validation"*. Journal of Composites Science 6, No. 3, pp 98, 2022.